Prediction and Discriminating Experiments for the Residual Clock–Energy Framework

CMB Transfer Templates, Phase-Clock Tests, Quantum Tunneling, Lapse-Map Diagnostics, and Boundary-Scar Scaling

Byoungwoo Lee
Independent Researcher
Daejeon, Republic of Korea

Version v0.4r1 – April 2026

Abstract

This note formulates a prediction and falsifiability layer for the Residual Clock–Energy framework. The purpose is not to add another theorem-polishing manuscript, nor to claim that an observed anomaly has already been detected. Instead, the note asks a concrete experimental question: if a single residual clock sector is physically meaningful, what cross-channel signatures should it generate, and how can those signatures be distinguished from independent nuisance effects in standard descriptions?

The starting point is the residual clock chain

$$\alpha = d\Phi - A \longrightarrow R_\alpha \longrightarrow L_\alpha \longrightarrow T \longrightarrow K_T,$$

where α is a residual phase-tension one-form, R_α is a residual drive or curvature proxy, L_α is a structural lapse, T is operational time, and K_T is the generator measured in that clock. A framework-specific prediction is not merely a new fit parameter in one data set. It is a compressed correlation: the same residual clock normalization should control, at least in a regime-dependent way, clock drift, dephasing, entropy production, CMB transfer morphology, microscopic tunneling response, lattice lapse-map structure, and boundary-scar scaling.

Version v0.4r1 is a minor-polished public protocol draft. It keeps the implementation layer of the preceding draft and performs a consistency cleanup for public release: old version residues are removed, the structural-time genealogy is synchronized, the abstract residual chain is unnumbered, the first tunneling-time observable is fixed explicitly as a phase-time/Wigner–Smith proxy, a boundary-layer lapse profile is added to clarify Hartman-like saturation logic, and the internal source-record citations are synchronized to the current public records. The manuscript still joins the five channels through a cross-channel residual consistency ledger, a falsifiability table, and a priority roadmap. All channels are framed conservatively as protocols, templates, and exclusion tests rather than as anomaly claims.

Contents

Introduction

The Residual Clock–Energy framework proposes that physical time, generator cost, phase relaxation, and residual structure are not always best treated as separable bookkeeping devices. Its core object is not a new force field in the ordinary sense, but a residual clock sector: a sector in which a phase-tension one-form, a lapse, an operational clock, and a measured generator are linked by a structural chain. In its minimal notation this chain is

$$\alpha = d\Phi - A \longrightarrow R_\alpha \longrightarrow L_\alpha \longrightarrow T \longrightarrow K_T \longrightarrow E_\alpha[T]. \tag{1}$$

Here α is the residual phase tension, R_α is a residual drive or curvature proxy, L_α is the induced structural lapse, T is operational time, K_T is the generator in that clock, and $E_\alpha[T]$ is the associated positive residual generator cost.

The previous source manuscripts in this line developed the conceptual and mathematical layers of this chain: the original structural-lapse intuition, the operational-time monograph, the minimal residual clock-energy coupling, the residual phase-relaxation arrow, and black-hole operational-time boundary applications. The present note has a different role. It asks what would make the framework testable. A physical framework can be internally coherent but still experimentally weak if every proposed signal can be absorbed into an unconstrained nuisance model. The central purpose of this note is therefore to identify signatures that are not isolated anomalies, but correlated predictions across multiple domains.

The organizing slogan is:

$$\boxed{\text{one residual clock sector} \quad \Longrightarrow \quad \text{multiple correlated signatures.}} \tag{2}$$

The channels considered in this note are

$$\begin{aligned} &\text{clock drift} \Longleftrightarrow \text{dephasing} \Longleftrightarrow \text{entropy production} \Longleftrightarrow \text{CMB morphology} \\ &\qquad \Longleftrightarrow \text{microscopic tunneling} \Longleftrightarrow \text{lapse-map structure} \Longleftrightarrow \text{boundary-scar scaling}. \end{aligned} \tag{3}$$

A standard model may explain one member of this chain by ordinary noise, another by a foreground residual, another by phase diffusion, and another by a detector artifact. The Residual Clock–Energy claim becomes experimentally sharper only if a common residual normalization, morphology, or scaling law is seen across more than one channel.

Claim posture

This manuscript is intentionally conservative in its claim posture. It does not claim that quantum mechanics is wrong, that a CMB anomaly has been detected, that the Hartman effect has been solved, that a black-hole scar has been observed, or that standard effective theory has been refuted. The correct reading is more precise:

- standard limiting results should be recovered in the appropriate regimes;
- residual clock-sector structure is added as an interpretation and correlation layer;
- the novel object is not a single anomaly, but a cross-channel covariance pattern;
- null results are valuable, because they bound the residual normalization and reduce the allowed parameter space;
- a successful test requires morphology, scaling, and co-variation that are difficult to mimic by independently tuned nuisance models.

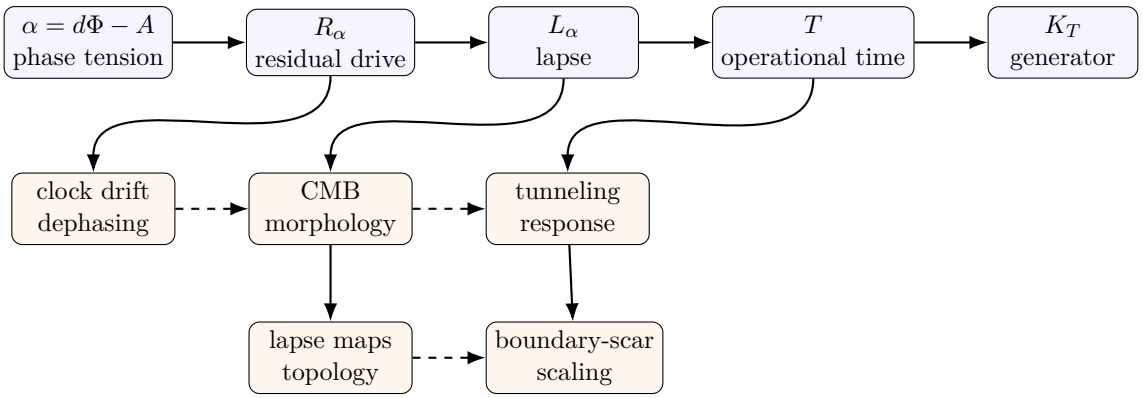

Figure 1: The prediction logic of this note. The residual clock chain is not tested by a single anomaly. It is tested by whether a common residual normalization produces correlated signatures across observational, laboratory, numerical, and boundary regimes.

How this note is organized

Section 1 states the purpose and the residual clock-generator principle. Section 2 defines what counts as a discriminating prediction, with emphasis on parameter compression, morphology, null tests, and cross-channel covariance. Section 3 develops the first prediction channel: a CMB residual clock-emergence feature, treated as a transfer-template and pseudo-likelihood program.

The continuation of the manuscript then proceeds through the remaining prediction channels: laboratory phase-clock tests, microscopic tunneling, lattice lapse maps, black-hole boundary-scar scaling, cross-channel consistency, the falsifiability ledger, and the priority roadmap.

Public protocol layer

The present public protocol draft adds an implementation layer to the prediction program. The main additions are: a small predeclared CMB template grid and binned likelihood convention; a laboratory error-budget model separating heating, technical phase noise, and residual drive; explicit nuisance-control operations; a Josephson/SQUID first-platform protocol; a fixed first tunneling-time observable for a primary tunneling protocol; code-facing lattice definitions and failure criteria; a synthetic boundary-scar catalog protocol; and a sharper residual-export rule for transporting channel constraints to a common scale. These additions are deliberately modest. They do not convert the note into an empirical claim. They make it harder for the framework to avoid null tests.

1 Purpose and Principle

The purpose of this note is to translate the Residual Clock–Energy framework into a set of discriminating predictions. The framework has already been developed as a structural account of residual phase tension, operational time, generator cost, entropy production, and boundary behavior. The present task is narrower: identify what an experimenter, simulator, or data analyst should measure if the framework is to become empirically constrained.

1.1 From structural lapse to residual clock sector

The genealogy begins with a structural-lapse intuition: physical evolution may be represented not only by a background coordinate time t, but also by an operational clock T related through a lapse factor,

$$\mathrm{d}T = L\ \mathrm{d}t. \tag{4}$$

In the original Degenerate-Time / structural-time language one also writes an effective structural generator of the form

$$H_s = \frac{H}{L}. \tag{5}$$

The Residual Clock–Energy framework refines this lapse idea by tying the lapse to a residual phase-sector variable rather than treating it as a free phenomenological clock factor.

The residual one-form is

$$\alpha = d\Phi - A, \tag{6}$$

where Φ is a phase field and A is a connection or gauge-like compensator. The point of (6) is not that every physical system literally contains the same microscopic field. It is that a mismatch between phase evolution and compensating structure can be represented by a residual tension. From this tension one extracts a residual drive or curvature proxy R_α, and from that drive one constructs a lapse L_α.

A convenient minimal parametrization is

$$L_\alpha = L_0 \exp\{-\mathcal{R}_\alpha\}, \qquad \mathcal{R}_\alpha \geq 0, \tag{7}$$

where $\mathcal{R}_\alpha$ denotes a nonnegative residual intensity functional. Other monotone lapse laws are possible, but (7) has two practical advantages: it preserves positivity and makes clock suppression multiplicative.

Remark 1.1 (Notation warning)**.** The residual one-form $\alpha = d\Phi - A$ should not be confused with unrelated phenomenological parameters that may also have been denoted by α in earlier Degenerate-Time / structural-time or lattice parametrizations. In this note, α always denotes the residual phase-tension one-form unless explicitly stated otherwise.

1.2 Operational time and the measured generator

Once a lapse L_α is specified, operational time is defined by

$$T(t) = T(t_0) + \int_{t_0}^{t} L_\alpha(s)\ \mathrm{d}s. \tag{8}$$

The generator measured with respect to this clock is written K_T. In simple scalar lapse models one expects the schematic relation

$$K_T \sim L_\alpha^{-1} H \tag{9}$$

with additional connection, domain, and ordering terms in more structured settings. The associated residual generator cost is represented by a nonnegative functional

$$E_\alpha[T] = \int_{T_0}^{T_1} \mathcal{E}_\alpha(\Phi, A, L_\alpha, K_T)\ \mathrm{d}T, \qquad E_\alpha[T] \geq 0. \tag{10}$$

The exact form of $\mathcal{E}_\alpha$ depends on the physical channel. In a phase-relaxation model it may be a gradient-flow cost. In a tunneling model it may appear as an opacity-linked clock suppression. In a CMB template it may enter as a residual transfer amplitude.

The prediction question is therefore not whether every system uses the same detailed $\mathcal{E}_\alpha$. The question is whether a common residual clock normalization can be transported across channels in a way that constrains data.

1.3 The residual prediction map

For the purposes of this note, a prediction channel is a map

$$\mathfrak{P}_j : (\mathcal{R}_{\rm clock}, \vartheta_j, \nu_j) \longmapsto \mathcal{O}_j, \tag{11}$$

where

- $\mathcal{R}_{\rm clock}$ is the shared residual clock normalization or residual scale;
- ϑ_j denotes channel-specific physical parameters;
- ν_j denotes nuisance parameters;
- $\mathcal{O}_j$ is the measured observable vector in channel j.

The framework becomes experimentally meaningful only if several $\mathfrak{P}_j$ share a common component of $\mathcal{R}_{\rm clock}$ in a way that is not removable by arbitrary nuisance redefinitions.

For example, the CMB channel may constrain a residual transfer amplitude $\epsilon_{\rm clock}$. A laboratory phase-clock channel may constrain a drift coefficient $\lambda_\nu \mathcal{R}_{\rm clock}$. A tunneling channel may constrain an opacity-to-clock response. None of these constraints alone is decisive. Their value lies in whether they can be placed on one residual scale ledger.

Diagnostic criterion 1.2 (One-sector compression)**.** A set of channels $\{j_1, \ldots, j_m\}$ is said to pass the one-sector compression test if there exists a residual scale $\mathcal{R}_{\rm clock}$ and channel maps $\mathfrak{P}_j$ such that the observed vectors $\mathcal{O}_j^{\rm obs}$ are jointly fit with fewer independent residual parameters than would be required by separate nuisance explanations, while preserving the predicted signs, morphologies, and scaling laws.

The above definition is deliberately statistical rather than metaphysical. It does not ask whether the residual sector has been ontologically confirmed. It asks whether the residual-sector representation compresses observations in a way that is predictive and falsifiable.

1.4 What would count as progress?

The realistic near-term goal is not a spectacular positive detection. It is a hierarchy of increasingly constraining tests:

(L1) **Template construction.** Build channel templates whose parameters are clearly tied to residual clock variables.

(L2) **Null-bound extraction.** Derive upper bounds on residual amplitudes from existing data or simple experiments.

(L3) **Controlled injection tests.** Inject synthetic residual signatures into mock data and recover them without bias.

(L4) **Cross-channel consistency.** Compare residual scales across channels under predeclared normalization conventions.

(L5) **Discriminating prediction.** Identify a sign, morphology, scaling law, or covariance relation that standard nuisance models can mimic only by independent tuning.

This progression is important because the Residual Clock–Energy framework is broad. A broad framework becomes scientifically useful only when it creates narrow tests.

2 What Counts as a Discriminating Prediction?

A discriminating prediction is not the same thing as a possible explanation. Almost any flexible model can be made to explain an observed feature after the fact. The relevant standard is stronger: a prediction should reduce freedom, not add arbitrary freedom.

2.1 Four failure modes

The following failure modes must be avoided.

Single-anomaly overfitting. A single residual in one data set is rarely decisive. A CMB feature can be a foreground artifact, a mask effect, a look-elsewhere fluctuation, or a parameter degeneracy. A tunneling-time anomaly can depend on which time definition is used. A dephasing drift can be ordinary technical noise. A boundary echo can be an analysis artifact. Therefore this note treats single-channel anomalies as hypothesis generators, not confirmations.

Unconstrained nuisance absorption. If every mismatch can be absorbed into a new nuisance function, the framework is not falsifiable. Each proposed residual parameter must have a declared role, dimensional scaling, and cross-channel expectation.

Loss of standard limits. A useful residual-clock model must recover standard baseline behavior when the residual scale is taken to zero. In the CMB channel this means returning to the baseline primordial spectrum and standard transfer calculation. In tunneling this means recovering the WKB opacity law. In laboratory phase-clock tests this means ordinary oscillator and dephasing behavior in the absence of a residual drive.

Ambiguous clock observables. Clock language is dangerous unless the observable is specified. In tunneling, for example, phase time, dwell time, Larmor-clock time, weak-measurement time, and detector response time are not interchangeable. A serious protocol must state which clock observable is being tested.

2.2 Criteria for a discriminating prediction

The following criteria will be used throughout this manuscript.

Diagnostic criterion 2.1 (Discriminating prediction criteria)**.** A proposed Residual Clock–Energy prediction is discriminating if it satisfies the following conditions.

(D1) **Baseline recovery.** The prediction reduces to a standard theory limit when the residual scale vanishes.

(D2) **Parameter compression.** The same residual normalization controls more than one observable, or more than one channel, with fewer degrees of freedom than independent nuisance fits.

(D3) **Morphological specificity.** The prediction has a shape, sign, scaling law, or covariance pattern not freely adjustable after the fact.

(D4) **Observable declaration.** The measured quantity is specified before the comparison is made.

(D5) **Null-test meaning.** A null result gives a bound on a residual amplitude, coupling, or morphology class.

(D6) **Cross-channel transport.** When possible, the residual scale inferred from one channel can be transported to another channel through a declared normalization map.

The criteria are intentionally severe. They are designed to prevent a broad conceptual framework from becoming an unfalsifiable explanatory language.

2.3 Residual covariance as the target object

The strongest experimental target is not the mean residual in one observable, but the covariance structure among observables. Let

$$\mathcal{O} = (\mathcal{O}_{\mathrm{CMB}}, \mathcal{O}_{\mathrm{phase}}, \mathcal{O}_{\mathrm{tun}}, \mathcal{O}_{\mathrm{lat}}, \mathcal{O}_{\mathrm{scar}}) \tag{12}$$

collect the CMB, laboratory phase-clock, tunneling, lattice lapse-map, and boundary-scar observables. A minimal residual model predicts that, after removal of channel-specific baselines,

$$\delta\mathcal{O}_j = \beta_j \mathcal{R}_{\mathrm{clock}} + \xi_j + O(\mathcal{R}^2_{\mathrm{clock}}), \tag{13}$$

where β_j is a channel response coefficient and ξ_j is a nuisance residual with declared covariance. In the simplest cross-channel test,

$$\mathrm{Cov}(\delta\mathcal{O}_i, \delta\mathcal{O}_j) \approx \beta_i\beta_j \,\mathrm{Var}(\mathcal{R}_{\mathrm{clock}}) + \mathrm{Cov}(\xi_i, \xi_j). \tag{14}$$

If the nuisance covariance is expected to be small or morphologically different, the residual clock sector predicts a sign and structure for cross-channel covariance.

Remark 2.2 (Why covariance matters)**.** A single channel can usually be explained away. Cross-channel covariance is harder to dismiss, especially when the channels have unrelated instrumental systematics. This is why the present note treats residual clock-energy as a correlation framework before treating it as a discovery claim.

2.4 Null results and parameter exclusion

A null result is not a failure if it narrows the residual sector. Each channel should produce a bound of the form

$$|\mathcal{R}_{\mathrm{clock}}| \le \mathcal{R}^{(j)}_{\mathrm{max}} \tag{15}$$

or, more generally,

$$|\beta_j \mathcal{R}_{\mathrm{clock}}| \le \Delta^{\mathrm{obs}}_j, \tag{16}$$

where Δ^{obs}_j is the channel's observational or experimental tolerance. The joint bound is then

$$|\mathcal{R}_{\mathrm{clock}}| \le \min_j \frac{\Delta^{\mathrm{obs}}_j}{|\beta_j|}, \tag{17}$$

provided the response coefficients have been normalized consistently.

This is the practical meaning of falsifiability for the present note. The framework becomes more scientific as the allowed residual sector becomes smaller, even before any positive detection.

2.5 Protocol hierarchy

Each prediction channel should be developed through a protocol ladder:

(P1) **Analytic template.** Write the residual deformation of the standard baseline.

(P2) **Synthetic injection.** Generate mock data with known residual amplitude and recover it.

(P3) **Nuisance stress test.** Add plausible foreground, noise, systematic, or model-degeneracy effects.

(P4) **Blind or predeclared fit.** Fit real data with a fixed template and declared priors.

(P5) **Cross-channel comparison.** Convert the inferred residual amplitude into a common ledger.

Sections 3–7 instantiate this ladder in specific domains. The present implementation draft begins this ladder explicitly in the CMB channel and then carries the same protocol logic through the laboratory, tunneling, lattice, and boundary-scar channels.

3 Prediction I: CMB Residual Clock-Emergence Feature

The CMB channel is the most natural first observational test because it probes the earliest accessible linear transfer surface of cosmological structure. It is also dangerous, because CMB data are highly model-dependent and systematics-sensitive. The correct use of the CMB in this note is therefore not to claim an anomaly. It is to define a residual clock-emergence template, propagate it through standard transfer functions, and ask what amplitude is allowed by temperature and polarization spectra.

3.1 Baseline and residual deformation

Let the baseline scalar curvature spectrum be the usual power-law form

$$P_\zeta^{(0)}(k) = A_s \left(\frac{k}{k_0}\right)^{n_s-1}. \tag{18}$$

A minimal residual clock-emergence deformation is represented by a localized logarithmic feature,

$$P_\zeta(k) = A_s \left(\frac{k}{k_0}\right)^{n_s-1} \left[1 + \epsilon_{\rm clock} \exp\left(-\frac{\log^2(k/k_*)}{2\sigma_*^2}\right)\right]. \tag{19}$$

Here $\epsilon_{\rm clock}$ is the residual clock-emergence amplitude, k_* is the feature scale, and σ_* is the logarithmic width. The residual interpretation is not that (19) is the only possible primordial feature. The interpretation is that it provides a controlled first template for translating a residual clock emergence into CMB observables.

A more general family may include oscillatory or asymmetric envelopes,

$$P_\zeta(k) = P_\zeta^{(0)}(k)\left[1 + \epsilon_{\rm clock}\, F_{\rm clock}(\log k; k_*, \sigma_*, \varphi, \rho)\right], \tag{20}$$

where $F_{\rm clock}$ is a predeclared shape function. For the present implementation draft, however, the log-Gaussian feature in (19) is preferable because it is simple, positive/negative according to the sign of $\epsilon_{\rm clock}$, and easy to inject into Boltzmann pipelines.

3.2 Transfer to angular spectra

The scalar CMB spectra are obtained schematically from

$$C_\ell^{XY} = 4\pi \int_0^\infty \frac{{\rm d}k}{k} P_\zeta(k) \Delta_\ell^X(k) \Delta_\ell^Y(k), \qquad X, Y \in \{T, E\}, \tag{21}$$

where Δ_ℓ^T and Δ_ℓ^E are the temperature and E-mode transfer functions. The residual clock feature induces

$$\delta C_\ell^{XY} = 4\pi \epsilon_{\rm clock} \int_0^\infty \frac{{\rm d}k}{k} P_\zeta^{(0)}(k) F_{\rm clock}(k) \Delta_\ell^X(k) \Delta_\ell^Y(k) + O(\epsilon_{\rm clock}^2). \tag{22}$$

Thus the observable CMB signature is not simply a bump in $P_\zeta(k)$, but a correlated pattern in

$$\delta \mathbf{C}_\ell = (\delta C_\ell^{\rm TT}, \delta C_\ell^{\rm TE}, \delta C_\ell^{\rm EE}). \tag{23}$$

The Residual Clock–Energy-specific part is the requirement that these three responses arise from the same residual amplitude and feature scale.

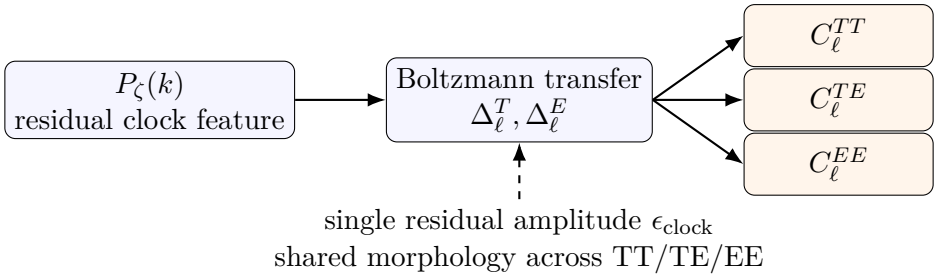

Figure 2: CMB residual clock-emergence test. The discriminating object is not an isolated temperature feature, but a shared TT/TE/EE morphology generated by one residual template.

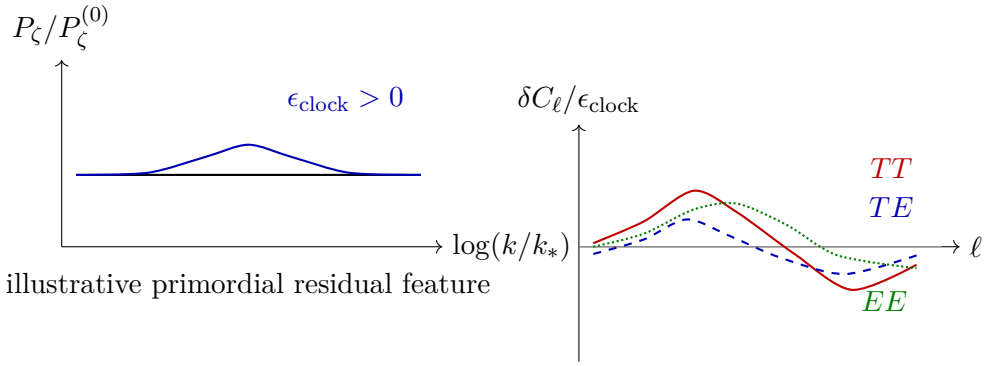

Figure 3: Illustrative schematic example of the CMB channel. Left: a localized residual clock-emergence feature in the primordial spectrum. Right: the induced response is not identical in TT, TE, and EE because the transfer functions project the same primordial feature into different acoustic and polarization morphologies. The curves are schematic and meant only to visualize the logic of the protocol.

3.3 Residual clock interpretation

The template (19) can be interpreted as a phenomenological projection of a clock-emergence event. Suppose that a residual lapse transition occurs around a characteristic scale k_*. A simple model is

$$L_{\rm clock}(k) = 1 - \eta_{\rm clock} \exp\left(-\frac{\log^2(k/k_*)}{2\sigma_*^2}\right), \tag{24}$$

with $|\eta_{\rm clock}| \ll 1$. If the curvature spectrum responds linearly to this transition, then

$$\epsilon_{\rm clock} \approx \lambda_\zeta \eta_{\rm clock}, \tag{25}$$

where λ_ζ is a channel response coefficient. The exact microscopic origin of λ_ζ is not fixed in this protocol note. What matters for the prediction program is that $\epsilon_{\rm clock}$ becomes the CMB ledger entry for the residual clock scale.

Prediction 3.1 (CMB residual clock-emergence feature)**.** A residual clock-emergence event projected onto the primordial curvature spectrum predicts a correlated deformation of C_ℓ^{TT}, C_ℓ^{TE}, and C_ℓ^{EE} controlled by a common parameter triple $(\epsilon_{\rm clock}, k_*, \sigma_*)$, up to standard cosmological and nuisance parameters. A positive indication requires not merely a localized improvement in one spectrum, but a predeclared TT/TE/EE transfer morphology consistent with the same residual feature.

3.4 Pseudo-likelihood and exclusion bound

Let $\mathbf{d}$ denote a vector of binned CMB observables and let

$$\mathbf{m}(\theta, \epsilon_{\rm clock}, k_*, \sigma_*) \tag{26}$$

be the theoretical vector, where θ denotes standard cosmological and nuisance parameters. A first pseudo-likelihood can be defined by

$$\chi^2(\theta, \epsilon_{\rm clock}, k_*, \sigma_*) = \big[\mathbf{d} - \mathbf{m}(\theta, \epsilon_{\rm clock}, k_*, \sigma_*)\big]^T \boldsymbol{\Sigma}^{-1} \big[\mathbf{d} - \mathbf{m}(\theta, \epsilon_{\rm clock}, k_*, \sigma_*)\big], \tag{27}$$

where $\boldsymbol{\Sigma}$ is an approximate covariance matrix. The profile statistic is

$$\Delta\chi^2(\epsilon_{\rm clock}, k_*, \sigma_*) = \min_{\theta} \chi^2(\theta, \epsilon_{\rm clock}, k_*, \sigma_*) - \min_{\theta,\epsilon,k,\sigma} \chi^2(\theta, \epsilon, k, \sigma). \tag{28}$$

A conservative null result gives a bound

$$|\epsilon_{\rm clock}| < \epsilon_{\rm max}(k_*, \sigma_*) \tag{29}$$

for each scale-width pair. This bound is already useful, because it becomes the CMB entry in the cross-channel residual ledger.

For an actual bandpower pass, the likelihood object should be written directly in binned spectra. Let D_b^{XY} denote binned spectra for $XY \in \{\mathrm{TT}, \mathrm{TE}, \mathrm{EE}\}$ and let

$$\Delta D_b^{XY}(\epsilon, k_*, \sigma_*) = D_{b,\rm obs}^{XY} - D_{b,\rm model}^{XY}(\widehat{\theta}, \epsilon, k_*, \sigma_*), \tag{30}$$

where $\widehat{\theta}$ is either fixed at the baseline best fit or profiled over declared nuisance/cosmological directions. The binned pseudo-likelihood is

$$\chi^2_{\rm bin}(\epsilon, k_*, \sigma_*) = \sum_{\substack{b,b' \\ XY,X'Y' \in \{\mathrm{TT,TE,EE}\}}} \Delta D_b^{XY} \left[\mathrm{Cov}^{-1}\right]_{bb'}^{XY,X'Y'} \Delta D_{b'}^{X'Y'}. \tag{31}$$

Equation (31) is the version that should be used in a public data-facing implementation, because it makes masking, binning, covariance, and nuisance projection explicit.

Protocol 3.2 (CMB transfer-template ladder)**.** The CMB prediction should be developed through the following ladder.

(CMB-1) **Synthetic transfer.** Inject (19) into a Boltzmann solver and compute δC_ℓ^{TT}, δC_ℓ^{TE}, and δC_ℓ^{EE}.

(CMB-2) **Recovery test.** Fit the injected spectra and verify unbiased recovery of $(\epsilon_{\rm clock}, k_*, \sigma_*)$.

(CMB-3) **Nuisance stress.** Add foreground, beam, calibration, lensing-amplitude, and masking nuisance deformations and quantify degeneracies.

(CMB-4) **Pseudo-likelihood.** Apply (27), the binned version (31), or a full public likelihood to obtain (29).

(CMB-5) **Ledger export.** Convert $\epsilon_{\rm max}$ into a residual clock bound using a declared response coefficient λ_ζ.

3.5 Discriminating morphology

A primordial feature produces different projections in TT, TE, and EE because the transfer functions have different acoustic phases and polarization response. Therefore a genuine residual clock-emergence template should not be judged by temperature alone. The morphology vector

$$\mathcal{M}_{\rm CMB}(k_*,\sigma_*) = \left(\frac{\delta C_\ell^{TT}}{\epsilon_{\rm clock}}, \frac{\delta C_\ell^{TE}}{\epsilon_{\rm clock}}, \frac{\delta C_\ell^{EE}}{\epsilon_{\rm clock}}\right)_{\ell\in\mathcal{L}} \tag{32}$$

should be precomputed for each template point. The key question is then whether the residual pattern projects coherently across spectra.

A useful morphology score is

$$\mathcal{S}_{\rm CMB} = \frac{\langle \delta\mathbf{C}^{\rm obs}, \mathcal{M}_{\rm CMB}\rangle_{\Sigma^{-1}}}{\sqrt{\langle \mathcal{M}_{\rm CMB}, \mathcal{M}_{\rm CMB}\rangle_{\Sigma^{-1}}}}, \tag{33}$$

where $\langle\cdot,\cdot\rangle_{\Sigma^{-1}}$ denotes covariance-weighted inner product after projection away from declared nuisance directions. A high score is not by itself a discovery; it is a trigger for cross-channel comparison.

3.6 Falsifiability in the CMB channel

Falsifiability test 3.3 (CMB null result)**.** For a fixed template family $F_{\rm clock}$ and a fixed analysis range $\mathcal{L}$, the CMB channel falsifies residual clock-emergence amplitudes satisfying

$$|\epsilon_{\rm clock}| > \epsilon_{\rm max}(k_*,\sigma_*) \tag{34}$$

whenever the corresponding TT/TE/EE morphology is absent after nuisance projection. The null result does not falsify the entire Residual Clock–Energy framework, but it excludes that template region and tightens the cross-channel residual ledger.

The important feature of Prediction 3.3 is that it makes the CMB channel useful even without a positive anomaly. A bound on $\epsilon_{\rm clock}$ restricts any later attempt to interpret laboratory or tunneling residuals as part of the same early-universe clock sector.

3.7 Template grid and design matrix

For a first reproducible pass, the template family should be reduced to a small grid rather than left as a free-form feature search. A useful first public grid is

$$k_* \in \{2\times10^{-3}, 10^{-2}, 5\times10^{-2}\}\,{\rm Mpc}^{-1}, \qquad \sigma_* \in \{0.15, 0.30, 0.60\}, \tag{35}$$

with both signs of $\epsilon_{\rm clock}$ tested. The exact grid may be modified in a later data-facing implementation, but a fixed grid prevents the first pass from becoming an unconstrained anomaly search.

For each grid point define the CMB response vector

$$\mathbf{g}_{ab} = \left.\frac{\partial \mathbf{m}(\theta,\epsilon_{\rm clock},k_*,\sigma_*)}{\partial\epsilon_{\rm clock}}\right|_{\epsilon_{\rm clock}=0,\ k_*=k_a,\ \sigma_*=\sigma_b}, \tag{36}$$

where $\mathbf{m}$ contains binned TT, TE, and EE spectra after the same masking, binning, and nuisance treatment used for the baseline model. The first-order template fit is then a one-parameter regression at each grid point:

$$\widehat{\epsilon}_{ab} = \frac{\mathbf{g}_{ab}^T\Sigma^{-1}\mathbf{r}_0}{\mathbf{g}_{ab}^T\Sigma^{-1}\mathbf{g}_{ab}}, \qquad \sigma^2_{\epsilon,ab} = \frac{1}{\mathbf{g}_{ab}^T\Sigma^{-1}\mathbf{g}_{ab}}, \tag{37}$$

where $\mathbf{r}_0 = \mathbf{d} - \mathbf{m}(\widehat{\theta},0)$ is the baseline residual vector. Nuisance projection can be implemented by replacing $\mathbf{g}_{ab}$ by its component orthogonal to the declared nuisance tangent space.

Table 1: Minimal CMB template-grid ledger for the first public pass. The output is not a discovery statistic by itself; it is a reproducible way to export a CMB bound to the residual clock ledger.

Grid object	Values / definition	Export
Feature scale	$k_* = 0.002, 0.010, 0.050\,\mathrm{Mpc}^{-1}$	scale localization of the residual clock-emergence template
Feature width	$\sigma_* \in \{0.15, 0.30, 0.60\}$	broadness of the logarithmic feature
Template sign	$\epsilon_{\mathrm{clock}} > 0$ and $\epsilon_{\mathrm{clock}} < 0$	clock-enhancement or suppression response
Design vector	$\mathbf{g}_{ab} = \partial_\epsilon \mathbf{m}\|_{0,k_a,\sigma_b}$	one-parameter TT/TE/EE morphology vector
Null export	$\|\epsilon_{ab}\| < N_\sigma \sigma_{\epsilon,ab}$	CMB residual-scale upper bound

3.8 Minimal deliverables for the next CMB pass

The next technical pass should produce four concrete deliverables:

(C1) a grid of template spectra δC_ℓ^{TT}, δC_ℓ^{TE}, δC_ℓ^{EE} for (k_*, σ_*);

(C2) injection-recovery plots for $\epsilon_{\mathrm{clock}}$;

(C3) a table of degeneracies with A_s, n_s, optical depth, lensing amplitude, foreground amplitude, and calibration parameters;

(C4) a preliminary exclusion surface $\epsilon_{\max}(k_*, \sigma_*)$.

These deliverables would convert the CMB section from a conceptual prediction into a reproducible diagnostic module.

4 Prediction II: Laboratory Residual Phase-Clock Test

The laboratory channel is the most direct place to test the residual clock-sector idea because it can be engineered, repeated, and null-tested. The target is not an exotic new force. The target is a correlation among frequency drift, dephasing, and dissipative entropy production under a controlled residual phase drive.

The relevant physical platforms include Josephson junctions and SQUIDs, superconducting phase circuits, Bose–Einstein condensates or superfluid phase-coherence systems, precision optical or microwave resonators, and high-stability oscillator comparisons. These systems already have standard descriptions. The residual clock-sector test is meaningful only if it recovers those standard descriptions at zero residual drive and then predicts a constrained co-variation when the residual phase tension is modulated.

4.1 Baseline phase variable and residual drive

Let $\phi(t)$ denote the experimentally accessible phase variable of a coherent system. The standard phase evolution may be represented schematically by

$$\dot{\phi}(t) = \omega_0 + \xi_0(t), \tag{38}$$

where ω_0 is the baseline angular frequency and ξ_0 is ordinary technical or thermal phase noise. A residual clock-sector deformation introduces a phase-tension variable

$$\alpha_{\mathrm{lab}}(t) = \dot{\Phi}(t) - A_t(t), \tag{39}$$

or, in a spatially extended phase medium,

$$\alpha_{\mathrm{lab}} = d\Phi - A. \tag{40}$$

The simplest residual intensity is

$$\mathcal{R}_{\mathrm{lab}}(t) = \langle |\alpha_{\mathrm{lab}}(t)|^2 \rangle_{\Omega}, \tag{41}$$

where the average is taken over the active region, device mode, or ensemble.

A minimal residual lapse law is then

$$L_{\mathrm{lab}}(t) = \exp\{-\lambda_L \mathcal{R}_{\mathrm{lab}}(t)\}, \qquad \lambda_L \geq 0. \tag{42}$$

For $\lambda_L \mathcal{R}_{\mathrm{lab}} \ll 1$,

$$L_{\mathrm{lab}}(t) = 1 - \lambda_L \mathcal{R}_{\mathrm{lab}}(t) + O(\mathcal{R}_{\mathrm{lab}}^2). \tag{43}$$

Thus the residual sector produces a small operational-time deformation.

4.2 Frequency drift, dephasing, and entropy production

If the measured frequency is the generator frequency with respect to operational time, then the first-order drift has the form

$$\frac{\delta\nu}{\nu} \simeq -\lambda_\nu \langle |\alpha_{\mathrm{lab}}|^2 \rangle, \tag{44}$$

with a platform-dependent response coefficient λ_ν. The sign convention in (44) reflects clock suppression: a positive residual intensity lowers the effective operational rate. A different device convention may reverse the reported sign, but the sign convention must be fixed before fitting.

The same residual drive should contribute to phase diffusion or dephasing. Let $X(t)$ denote the residual drive channel coupled to the phase. A coarse dephasing contribution is

$$\Gamma_{\mathrm{res}} \simeq \lambda_\Gamma \int_0^{\tau_m} \int_0^{\tau_m} \langle X(\tau) X(\tau') \rangle W(\tau, \tau') \, \mathrm{d}\tau \, \mathrm{d}\tau', \tag{45}$$

where W is the protocol-dependent filter kernel and τ_m is the measurement window. In a relaxation formulation the same sector also generates positive entropy production,

$$\Delta S_{\mathrm{res}} = \gamma \int_{T_0}^{T_1} |\mathrm{grad}\, \mathcal{A}_{\mathrm{res}}|_{h_T}^2 \, \mathrm{d}T, \qquad \gamma \geq 0. \tag{46}$$

Equations (44)–(46) are not intended as universal microscopic laws. They are a first response ledger: frequency drift, dephasing, and entropy production should not vary independently if they are driven by a common residual clock sector.

Prediction 4.1 (Laboratory phase-clock covariance)**.** Under a controlled residual phase drive, the measured frequency drift, residual dephasing rate, and dissipative entropy proxy should co-vary according to a common residual intensity $\mathcal{R}_{\mathrm{lab}}$. A positive indication is not a nonzero drift alone, but a reproducible covariance pattern

$$\mathcal{R}_{\mathrm{lab}} \longmapsto \left(\frac{\delta\nu}{\nu}, \Gamma_{\mathrm{res}}, \Delta S_{\mathrm{res}} \right) \tag{47}$$

with predeclared signs, response coefficients, and filter dependence.

4.3 Candidate experimental platforms

Josephson junctions and SQUIDs. The superconducting phase difference across a junction is a natural phase-clock variable. A residual clock protocol may modulate bias, flux, or environmental phase drive and compare critical current fluctuations, linewidth, phase diffusion, and frequency shift. The baseline is the Josephson relation and standard phase-diffusion theory [14, 15, 16]. The residual prediction is that a residual phase drive changes frequency drift and dephasing through a common response scale.

Protocol 4.2 (Josephson/SQUID residual phase-clock box)**.** For a first concrete platform, take the dimensionless flux-bias control

$$u = \frac{\Phi_{\mathrm{ext}}}{\Phi_0}, \qquad \Phi_0 = \frac{h}{2e}. \tag{48}$$

The gauge-invariant superconducting phase difference may be represented schematically by

$$\varphi = \phi_1 - \phi_2 - \frac{2\pi}{\Phi_0}\int_1^2 A \cdot d\ell, \tag{49}$$

so this platform is naturally aligned with the residual one-form logic $\alpha = d\Phi - A$. The concrete output map is

$$u \longmapsto \left(I_c(u),\ \Gamma_\phi(u),\ \frac{\delta\nu_{\mathrm{osc}}}{\nu_{\mathrm{osc}}}(u),\ S_{\phi\phi}(\omega; u) \right). \tag{50}$$

The residual test is not whether one of these four observables changes with flux bias. That is already expected in ordinary Josephson physics. The test is whether the residual components after baseline subtraction co-vary with a single intensity

$$\mathcal{R}_J(u) = \left\langle |\alpha_J(u)|^2 \right\rangle \tag{51}$$

under sign reversal, dummy-device controls, and noise-spectrum decomposition.

Superconducting phase circuits. Qubit or resonator circuits allow repeated coherent control, Ramsey-style dephasing measurements, and engineered noise injection. The advantage is protocol control; the danger is ordinary noise complexity. The residual test must therefore use control channels with identical standard noise budgets but different predicted residual coupling.

BEC and superfluid phase coherence. In a condensate or superfluid, the phase field is spatially extended. This makes (40) directly meaningful. The observable may be phase-coherence decay, vortex-linked phase relaxation, or interference contrast drift.

Precision oscillator comparisons. High-stability optical or microwave clocks provide strong null tests. The residual framework does not require immediate detection here; a null bound on a residual phase-clock coupling is already valuable.

4.4 A minimal lab protocol

Protocol 4.3 (Residual phase-clock laboratory ladder)**.** A first laboratory phase-clock test should proceed as follows.

(LAB-1) **Choose a phase-clock observable.** Predeclare whether the primary clock variable is oscillator frequency, Ramsey phase, Josephson frequency, resonator phase, or condensate interference phase.

(LAB-2) **Establish the baseline.** Fit the standard drift, diffusion, dissipation, and thermal-noise model without residual terms.

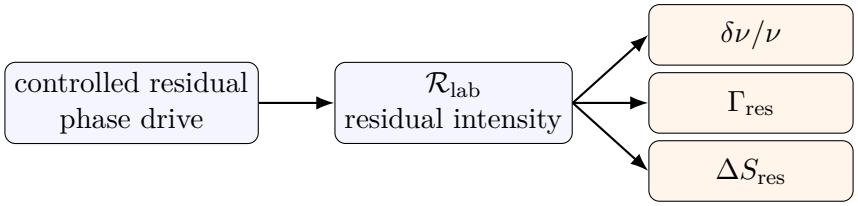

Figure 4: Laboratory phase-clock test. The discriminating object is the common covariance among drift, dephasing, and entropy proxy under a controlled residual phase drive.

Table 2: Illustrative laboratory export map for the residual phase-clock channel. The table is not a claim that all platforms are equally sensitive. Its purpose is to make the measurement vector more concrete.

Platform	Phase-clock observable	Dephasing / noise proxy	Entropy / dissipation proxy
Josephson junction / SQUID	Josephson frequency, phase difference, linewidth	phase diffusion, flux-noise response	bias-power dissipation, switching statistics
Superconducting circuit	Ramsey phase, resonator frequency	T_2^{-1}, spectral phase noise	excess heating, irreversible relaxation proxy
BEC / superfluid	interference phase, fringe contrast	coherence decay, vortex-induced relaxation	condensate damping, mode-population imbalance
Precision oscillator pair	fractional frequency shift $\delta\nu/\nu$	Allan deviation residuals, phase-noise spectrum	effective irreversible drift proxy

(LAB-3) **Inject a controlled residual drive.** Introduce a modulation expected to change $\mathcal{R}_{\mathrm{lab}}$ while keeping ordinary heating and technical noise monitored.

(LAB-4) **Measure the covariance vector.** Record $(\delta\nu/\nu, \Gamma_{\mathrm{res}}, \Delta S_{\mathrm{res}})$ or their platform-specific proxies.

(LAB-5) **Reverse or null the drive.** Use sign reversal, phase scrambling, or geometry reversal to distinguish residual phase tension from ordinary power injection.

(LAB-6) **Export a bound.** If no covariance is observed, report bounds on $\lambda_\nu \mathcal{R}_{\mathrm{lab}}$ and $\lambda_\Gamma \mathcal{R}_{\mathrm{lab}}$.

4.5 Null result

Falsifiability test 4.4 (Laboratory null result)**.** For a declared platform, filter function, and residual-drive protocol, absence of correlated drift–dephasing–entropy response gives

$$|\lambda_\nu \mathcal{R}_{\mathrm{lab}}| \le \Delta_\nu, \qquad |\lambda_\Gamma \mathcal{R}_{\mathrm{lab}}| \le \Delta_\Gamma, \tag{52}$$

where Δ_ν and Δ_Γ are experimental tolerances after baseline subtraction. This excludes the tested residual coupling region. It does not exclude all residual clock-sector models.

Table 3: Minimal nuisance-control and error-budget table for the laboratory phase-clock channel. A residual claim is admissible only after these ordinary effects are either subtracted, bounded, or shown to have the wrong symmetry or morphology.

Nuisance source	Control operation	Residual discriminator
Heating	temperature sweep; matched-power injection	residual component follows phase geometry or bias parity, not heat load
Technical phase noise	dummy resonator; off-resonant channel	absent or strongly suppressed in residual-insensitive channel
Electromagnetic pickup	shielding; cable reversal; ground-path swap	does not obey the declared phase-bias sign rule
Bias-current drift	interleaved baseline runs; randomized drive order	no covariance with the declared residual drive after baseline subtraction
Flux noise	sign reversal; gradiometric SQUID; reference loop	residual component has the predicted parity under $u \mapsto -u$
Device aging	repeated zero-drive calibration; run-order randomization	slow monotone drift does not mimic on/off residual covariance

5 Prediction III: Microscopic Quantum Tunneling as a Barrier-Clock Diagnostic

Quantum tunneling is a useful diagnostic because it already contains a tension between spatial propagation, amplitude suppression, phase response, and time observables. The Residual Clock–Energy framework should not be presented as a replacement for standard tunneling theory. The standard WKB opacity law must be recovered first. The residual contribution is an interpretation and correlation layer: an opaque barrier may be treated as a clock-suppressed or clock-degenerate sector, and the framework predicts correlated changes among transmission, traversal-time proxy, phase noise, dephasing, and frequency response.

5.1 Baseline WKB recovery

Consider a one-dimensional barrier $V(x) > E$ for $x \in [x_1, x_2]$. The standard WKB decay rate is

$$\kappa(x) = \frac{\sqrt{2m(V(x) - E)}}{\hbar}, \tag{53}$$

and the barrier opacity is

$$\mathcal{R}_B = \int_{x_1}^{x_2} \kappa(x)\, \mathrm{d}x. \tag{54}$$

The leading transmission law is

$$\mathcal{T} \sim e^{-2\mathcal{R}_B}. \tag{55}$$

This is the mandatory baseline. Any residual clock interpretation that fails to recover (55) in the ordinary limit should be rejected.

5.2 Barrier-clock reinterpretation

The residual clock reading treats the classically forbidden region not as a superluminal path, but as a clock-suppressed sector. A minimal local operational lapse inside the barrier is

$$L_{\mathrm{tun}}^{\mathrm{loc}}(x) = \exp\{-R_{\mathrm{tun}}(x)\}, \qquad R_{\mathrm{tun}}(x) \simeq c_B \kappa(x) \ell_B, \tag{56}$$

where ℓ_B is a local barrier length scale and c_B is a normalization constant. This local expression captures opacity suppression but, by itself, does not explain saturation with increasing barrier width.

For a Hartman-like saturation diagnostic, the public protocol draft therefore uses an explicit boundary-layer clock profile. Define the optical distance to the nearest barrier edge by

$$\rho_B(x) = \min\left\{\int_{x_1}^{x} \kappa(u)\ \mathrm{d}u, \int_{x}^{x_2} \kappa(u)\ \mathrm{d}u\right\}, \tag{57}$$

and set

$$L_{\mathrm{tun}}(x) = \exp\{-\rho_B(x)\}. \tag{58}$$

The accumulated operational barrier clock is then

$$\Delta T_{\mathrm{op}} \sim \int_{x_1}^{x_2} L_{\mathrm{tun}}(x)\ \mathrm{d}x. \tag{59}$$

For a uniform opaque barrier with constant κ and width $a = x_2 - x_1$,

$$\int_{x_1}^{x_2} e^{-\rho_B(x)}\ \mathrm{d}x = \frac{2}{\kappa}\left(1 - e^{-\kappa a/2}\right), \tag{60}$$

which saturates as $a \to \infty$. This gives a residual-clock reinterpretation of saturation-type traversal-time behavior without claiming that the Hartman effect has been solved in all definitions of tunneling time [10, 13].

Remark 5.1 (Tunneling-time caution)**.** There is no unique tunneling time. Phase time, dwell time, Larmor-clock time, weak-measurement time, and detector response time are distinct observables. A barrier-clock prediction is meaningful only after one of these observables is explicitly selected.

For the first implementation pass, the primary traversal-time observable is fixed to the phase-time/Wigner–Smith proxy

$$\tau_\varphi(E) = \hbar \frac{\partial}{\partial E} \arg t(E), \tag{61}$$

where $t(E)$ is the complex transmission amplitude. Dwell time and Larmor-clock time are treated as secondary cross-checks, not as interchangeable definitions of the primary clock observable.

5.3 Observable classes

For a tunneling platform, define the observable vector

$$\mathcal{O}_{\mathrm{tun}} = \left(\mathcal{T}, \tau_{\mathrm{op}}, S_{\phi\phi}^{\mathrm{res}}, \Gamma_{\mathrm{deph}}, \frac{\delta\nu}{\nu}\right). \tag{62}$$

Here $\mathcal{T}$ is transmission probability, τ_{op} is the declared traversal-time proxy, $S_{\phi\phi}^{\mathrm{res}}$ is residual phase-noise spectral density, Γ_{deph} is dephasing, and $\delta\nu/\nu$ is any clock or oscillator shift associated with the tunneling element.

The residual clock prediction is a constrained map

$$\mathcal{R}_B \longmapsto \left(\mathcal{T}, \tau_{\mathrm{op}}, S_{\phi\phi}^{\mathrm{res}}, \Gamma_{\mathrm{deph}}, \frac{\delta\nu}{\nu}\right), \tag{63}$$

where the first component must satisfy (55), and the remaining components should scale with the same opacity ledger.

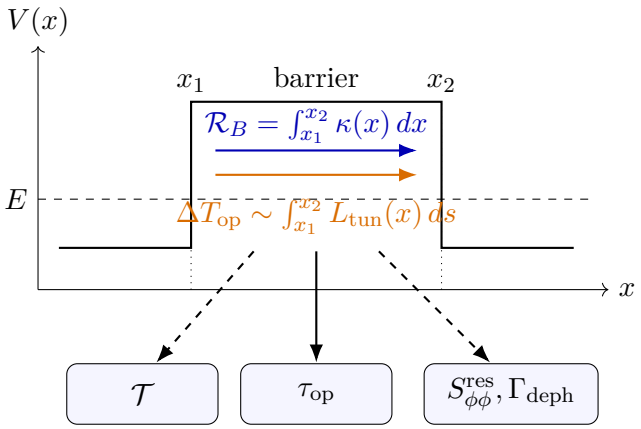

Figure 5: Barrier-clock schematic for the tunneling channel. The classically forbidden region is read as a clock-suppressed sector rather than as a superluminal path. The same opacity ledger $\mathcal{R}_B$ should govern not only transmission but also the chosen traversal-time proxy and any residual phase-noise/dephasing export.

Prediction 5.2 (Barrier-clock opacity correlation)**.** If a tunneling barrier acts as a residual clock-suppressed sector, then increasing opacity $\mathcal{R}_B$ should not merely suppress transmission. It should also produce a linked response in the declared traversal-time proxy, phase-noise spectrum, dephasing rate, and any coupled frequency shift. The framework-specific signature is the joint opacity dependence, not an isolated tunneling-time anomaly.

5.4 Experimental platforms

Scanning tunneling microscopy. In STM, the transmission current depends exponentially on tip-sample separation. A first residual diagnostic can compare $d \log I/dz$ with phase-noise and dwell-time proxies under controlled barrier changes. The null test asks whether opacity changes alter only current, or whether they also co-vary with residual phase-clock observables.

Josephson junctions and SQUIDs. A Josephson tunnel junction provides both a tunneling element and a phase-clock variable. The measurable quantities include critical current, phase diffusion, linewidth, flux response, and frequency shift. This is one of the most natural places to connect Section 4 and Section 5.

For the tunneling-specific Josephson/SQUID pass, the recommended observable vector is

$$\mathcal{O}_{J,\mathrm{tun}}(u) = \left(I_c(u),\ \Gamma_\phi(u),\ \frac{\delta\nu_{\rm osc}}{\nu_{\rm osc}}(u),\ S_{\phi\phi}(\omega; u),\ \tau_\varphi(u) \right). \tag{64}$$

The baseline Josephson/SQUID model may predict flux dependence in several components. The residual-clock test is the stricter residual covariance question: after subtracting the ordinary flux-response model, do the remaining components co-vary with a single residual drive u or $\langle |\alpha_J|^2 \rangle$?

Resonant tunneling diodes. Resonant tunneling devices allow barrier-width, voltage, and resonance-control studies. The residual-clock target is not a correction to every current-voltage feature, but a saturation or boundary-layer response in a declared time or noise proxy as opacity is increased.

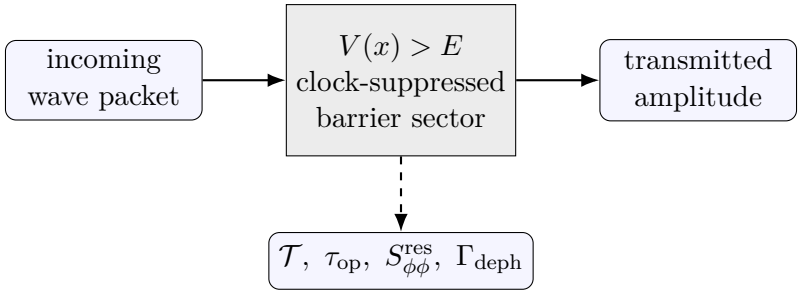

Figure 6: Barrier-clock diagnostic. The standard WKB transmission law is retained, while the residual hypothesis concerns opacity-linked clock, noise, and dephasing proxies.

5.5 Protocol

Protocol 5.3 (Barrier-clock tunneling protocol)**.** A microscopic tunneling test should proceed as follows.

(TUN-1) **Fix the first-pass traversal observable.** For the first public implementation, take $\tau_\varphi(E) = \hbar\partial_E \arg t(E)$ as the primary observable; record dwell time and Larmor-clock time only as secondary cross-checks.

(TUN-2) **Verify WKB baseline.** Confirm the transmission scaling $\mathcal{T} \sim e^{-2\mathcal{R}_B}$ in the selected parameter range.

(TUN-3) **Vary opacity.** Change barrier width, height, bias, or effective mass while monitoring heating and environmental noise.

(TUN-4) **Measure the joint response.** Record $\mathcal{T}$, $\tau_{\rm op}$, $S^{\rm res}_{\phi\phi}$, $\Gamma_{\rm deph}$, and any frequency shift.

(TUN-5) **Test boundary-layer saturation.** Determine whether $\tau_{\rm op}$ or phase-noise response saturates in the opaque regime while transmission continues to decay.

(TUN-6) **Export the opacity ledger.** Convert the result into bounds on barrier-clock response coefficients.

5.6 Null result

Falsifiability test 5.4 (Tunneling null result)**.** For a declared tunneling-time observable and barrier family, absence of any opacity-linked response beyond ordinary transmission gives

$$|\lambda_\tau \mathcal{R}_B| \le \Delta_\tau, \qquad |\lambda_\phi \mathcal{R}_B| \le \Delta_\phi, \qquad |\lambda_\Gamma \mathcal{R}_B| \le \Delta_\Gamma. \tag{65}$$

This excludes the tested barrier-clock response class. It does not imply that standard tunneling theory is wrong; rather, it reports that no residual barrier-clock signature was found in the tested observable.

6 Prediction IV: Lattice Lapse-Map Diagnostic

The lattice channel is a numerical diagnostic bridge between local residual structure and field-theoretic geometry. Its advantage is that fields, action density, topological charge density, and smoothing or flow-time dependence can be measured directly in an ensemble. Its danger is that ordinary action-density structures can mimic many apparent residual maps. Therefore the lapse-map diagnostic must explicitly separate residual topology/lapse correlation from ordinary energy-density correlation.

6.1 Residual energy map and lapse map

Let $R_E(x,\tau)$ be a residual energy or residual structure map at lattice site x and flow time τ. A minimal lapse map is

$$R_E(x,\tau) \longmapsto L_E(x,\tau) = L_0 \exp\{-R_E(x,\tau)\}. \tag{66}$$

The local clock suppression is strongest where R_E is large. If $q(x,\tau)$ denotes a topological charge-density proxy and $s(x,\tau)$ denotes action density, the discriminating question is whether L_E correlates with topological structure after conditioning on action density.

A simple conditional statistic is

$$\mathcal{C}_{Lq|s}(\tau) = \mathrm{Corr}\big(L_E(x,\tau), q(x,\tau) \mid s(x,\tau)\big), \tag{67}$$

or, more robustly, a rank or mutual-information statistic. The residual prediction is not merely that low lapse appears where action density is high. That would be expected. The residual prediction is that low-lapse structure carries topology-sensitive information not reducible to local action density alone.

Prediction 6.1 (Lapse-topology residual correlation)**.** A residual lattice lapse map should exhibit stable low-lapse regions whose distribution correlates with topological lumps or topological-charge structure after controlling for local action density and flow-time artifacts. The framework-specific signature is a stable conditional topology/lapse correlation, not simply a visual overlap between energy density and low lapse.

6.2 Flow-time stability

Gradient flow or cooling can suppress ultraviolet noise and reveal coherent structures. Let τ denote flow time. A stable residual lapse-map feature should satisfy a persistence condition over a predeclared flow-time window,

$$\mathcal{P}_L(\tau_1,\tau_2) = \frac{|\Omega_L(\tau_1) \cap \Omega_L(\tau_2)|}{|\Omega_L(\tau_1) \cup \Omega_L(\tau_2)|}, \tag{68}$$

where

$$\Omega_L(\tau) = \{x : L_E(x,\tau) \le L_{\mathrm{cut}}(\tau)\}. \tag{69}$$

The persistence threshold should be calibrated on null ensembles or shuffled topology labels. A strong signal is not merely persistence; it is persistence plus topology-conditioned information.

6.3 Ensemble-level universality

A useful lapse-map diagnostic should not be tied to a single hand-selected configuration. It should produce ensemble-level distributions:

$$\mathcal{D}_{\mathrm{lat}} = \Big\{P(L_E), \quad P(R_E), \quad P(\mathcal{C}_{Lq|s}), \quad P(\mathcal{P}_L), \quad P(\chi_{\mathrm{block}})\Big\}, \tag{70}$$

where χ_{block} denotes a block-level topological or residual susceptibility proxy. The residual clock-sector interpretation becomes stronger if these distributions show scaling stability across lattice spacing, volume, flow time, and action choices.

6.4 Protocol

Protocol 6.2 (Lattice lapse-map protocol)**.** A first lattice diagnostic should use the following ladder.

(LAT-1) **Define the residual map.** Specify $R_E(x,\tau)$ before inspecting configurations.

(LAT-2) **Construct the lapse map.** Use (66) or another declared monotone map.

(LAT-3) **Measure topology controls.** Compute $q(x,\tau)$, $s(x,\tau)$, block charges, and smoothing dependence.

(LAT-4) **Condition on action density.** Test whether L_E carries topology information beyond $s(x,\tau)$.

(LAT-5) **Test flow stability.** Measure (68) across a flow-time window.

(LAT-6) **Compare null ensembles.** Use shuffled labels, randomized phases, or matched action-density controls.

(LAT-7) **Export a residual map statistic.** Report $\mathcal{C}_{Lq|s}$, persistence, and ensemble distribution bounds.

Algorithm LAT-v0.4 (illustrative pseudocode)
Input: gauge ensemble U, flow window $[\tau_{\min}, \tau_{\max}]$, residual-map rule R_E, low-lapse threshold rule L_{cut}.
For each configuration U_n:
1. flow U_n to each τ in the declared grid;
2. compute action density $s(x,\tau)$ and topology proxy $q(x,\tau)$;
3. construct $R_E(x,\tau)$ and $L_E(x,\tau) = L_0 e^{-R_E(x,\tau)}$;
4. define low-lapse region $\Omega_L(\tau) = \{x : L_E(x,\tau) \le L_{\text{cut}}(\tau)\}$;
5. evaluate conditional statistic $\mathcal{C}_{Lq|s}(\tau)$;
6. evaluate persistence $\mathcal{P}_L(\tau_i, \tau_j)$;
7. repeat with null controls (shuffled q, matched s, randomized phase labels).

Aggregate over the ensemble and export:
$P(\mathcal{C}_{Lq|s})$, $P(\mathcal{P}_L)$, $P(L_E)$, $P(R_E)$, and $P(\chi_{\text{block}})$.

6.5 Sharp failure criteria

For the lattice channel, a failed realization should be stated before inspecting favorable plots. Two minimal targets are

$$\mathcal{C}_{L,q^2|s}(\tau) = \mathrm{Corr}\big(L_E(x,\tau), q(x,\tau)^2 \mid s(x,\tau)\big) \tag{71}$$

and a mutual-information target

$$\mathcal{I}_{L;q}(\tau) = I\big(L_E(x,\tau); q(x,\tau)\big), \tag{72}$$

with matched action-density controls. A tested lapse-map realization fails if, over the predeclared flow-time window $\mathcal{W}_\tau$, either

$$\sup_{\tau \in \mathcal{W}_\tau} \left|\mathcal{C}_{L,q^2|s}(\tau)\right| \le c_{\text{null}} \tag{73}$$

or

$$\sup_{\tau \in \mathcal{W}_\tau} \mathcal{I}_{L;q}(\tau) \le I_{\text{null}} \tag{74}$$

relative to shuffled-topology and matched-action null ensembles. It also fails if the persistence statistic $\mathcal{P}_L(\tau_i, \tau_j)$ is unstable across the declared flow-time window. This sharper rule prevents isolated visual coincidences from being counted as lapse-map evidence.

6.6 Null result

Falsifiability test 6.3 (Lattice null result)**.** If low-lapse regions are fully explained by local action density, fail to persist under the declared flow window, or show no topology-conditioned information relative to null ensembles, then the tested lattice lapse-map model is excluded. The null result bounds the map construction $R_E \mapsto L_E$ and prevents the framework from claiming arbitrary visual structure as a residual clock signature.

7 Prediction V: Black-Hole Boundary-Scar Scaling

The black-hole boundary channel is the most speculative of the five prediction channels. It should be treated as a scaling and classification protocol, not as a claim that post-ringdown residuals have already been detected. The purpose is to define what the residual clock-energy framework would predict if an operational-time boundary leaves a measurable scar in late-time gravitational-wave or horizon-sector data.

7.1 Regulated boundary generator

A schematic regulated boundary generator is

$$\widehat{K}_{T,\varepsilon} = (\widehat{L} + \varepsilon I)^{-1/2} \widehat{H} (\widehat{L} + \varepsilon I)^{-1/2}, \qquad \varepsilon > 0. \tag{75}$$

Here $\widehat{L}$ is a lapse operator or clock-suppression operator, $\widehat{H}$ is a baseline structural generator, and ε regularizes the lapse-degenerate boundary. The residual interpretation is that boundary-near lapse collapse can renormalize the generator and leave a finite residual boundary class.

The observational translation must be modest. If a residual ringdown feature or echo-like component is reported, the framework-specific question is not whether it exists in one event. The question is whether its dimensionless timing, damping, and morphology cluster according to a mass/spin-scaled boundary class.

7.2 Dimensionless scar time

Let M_f and a_f denote final black-hole mass and dimensionless spin, and let $t_{\rm scar}$ denote a declared post-ringdown residual time scale. Define

$$\Theta_{\rm scar} = \frac{c^3 t_{\rm scar}}{G M_f}. \tag{76}$$

A spin-refined version is

$$\Theta^{(a)}_{\rm scar} = \frac{c^3 t_{\rm scar}}{G M_f} F_a(a_f), \tag{77}$$

where F_a is a predeclared spin correction. The residual clock-sector prediction is clustering in $\Theta_{\rm scar}$ or $\Theta^{(a)}_{\rm scar}$, not an arbitrary event-by-event echo delay.

Prediction 7.1 (Boundary-scar scaling)**.** If operational-time boundary scars are physically present in a black-hole ringdown channel, their residual time scales should cluster after conversion to dimensionless mass/spin variables such as (76) or (77). The framework-specific signature is cross-event scaling stability, not a single low-significance residual feature.

7.3 Observable vector

A minimal scar observable vector is

$$\mathcal{O}_{\rm scar} = \left(\Theta_{\rm scar}, Q_{\rm scar}, A_{\rm scar}/A_{\rm rd}, \varphi_{\rm scar}, \mathcal{M}_{\rm scar}\right), \tag{78}$$

where $Q_{\rm scar}$ is a damping or quality proxy, $A_{\rm scar}/A_{\rm rd}$ is amplitude relative to ringdown, $\varphi_{\rm scar}$ is phase, and $\mathcal{M}_{\rm scar}$ is a morphology score against a predeclared template.

The residual clock-energy interpretation imposes a compression condition: events with similar boundary class should not require unrelated scar parameters.

For synthetic-catalog tests, the catalog record should be explicit rather than implicit. A minimal event-level field list is

$$\mathcal{C}^{\rm syn}_{\rm scar} = \{M_f, a_f, t_{\rm scar}, A_{\rm scar}/A_{\rm rd}, Q_{\rm scar}, \mathcal{M}_{\rm scar}, \text{noise seed}\}. \tag{79}$$

The purpose of (79) is not to claim observational evidence, but to make injection-recovery, false-positive, and cross-event clustering tests reproducible.

Table 4: Toy scaling ledger for the boundary-scar channel. The entries are illustrative organizing targets rather than fitted results. The point is to predeclare what kind of cross-event clustering would count as framework-relevant.

Quantity	Dimensionless form	Diagnostic meaning
Scar onset time	$\Theta_{\rm scar} = c^3 t_{\rm scar}/(GM_f)$	tests mass-scaled clustering of post-ringdown residual timing
Spin-refined onset	$\Theta^{(a)}_{\rm scar} = \Theta_{\rm scar} F_a(a_f)$	checks whether spin compresses the event cloud more effectively
Relative amplitude	$A_{\rm scar}/A_{\rm rd}$	tracks how strong any residual component is compared with ordinary ringdown
Quality / damping	$Q_{\rm scar}$	measures whether a candidate scar class has a coherent damping family
Morphology score	$\mathcal{M}_{\rm scar}$	compares residuals against one predeclared scar template rather than ad hoc fitting

7.4 Protocol

Protocol 7.2 (Boundary-scar scaling protocol)**.** A conservative black-hole boundary-scar test should proceed as follows.

(BH-1) **Predeclare the residual template.** Fix the post-ringdown time window, morphology class, and background ringdown subtraction method.

(BH-2) **Use injection studies.** Verify recovery and false-positive rates on synthetic data with known scar injections and realistic noise.

(BH-3) **Convert to dimensionless variables.** Report $\Theta_{\rm scar}$ and spin-refined variants rather than raw time delays.

(BH-4) **Test cross-event clustering.** Ask whether residual candidates cluster in the dimensionless scar ledger.

(BH-5) **Compare noise and analysis artifacts.** Stress-test against waveform systematics, detector glitches, and look-elsewhere choices.

(BH-6) **Export bounds.** If no scar class appears, bound the accessible amplitude and timing class.

7.5 Null result

Falsifiability test 7.3 (Boundary-scar null result)**.** Failure to observe a stable mass/spin-scaled scar class rules out the tested boundary-scar template above the accessible amplitude threshold. It does not rule out all boundary residuals, but it prevents arbitrary post-ringdown residuals from being interpreted as framework support without scaling compression.

8 Cross-Channel Residual Consistency

The strongest test of the Residual Clock–Energy framework is cross-channel consistency. Each individual channel can be criticized: CMB templates may be degenerate with foregrounds or primordial features; lab drift may be technical noise; tunneling-time data may depend on observable definition; lattice maps may reflect action-density artifacts; ringdown residuals may be noise. The framework becomes nontrivial only when a common residual scale explains more than one channel with fewer degrees of freedom than independent nuisance explanations.

8.1 Residual scale ledger

Let the shared residual scale be $\mathcal{R}_{\rm clock}$. Each channel exports a measured or bounded response

$$\rho_j = \beta_j \mathcal{R}_{\rm clock} + \eta_j, \tag{80}$$

where β_j is a response coefficient and η_j is channel-specific nuisance residue. For the five channels of this note,

$$\begin{aligned} \rho_{\rm CMB} &= \epsilon_{\rm clock}, \\ \rho_{\rm lab} &= (\delta\nu/\nu, \Gamma_{\rm res}, \Delta S_{\rm res}), \\ \rho_{\rm tun} &= \left(\tau_{\rm op}, S^{\rm res}_{\phi\phi}, \Gamma_{\rm deph}\right), \\ \rho_{\rm lat} &= \left(\mathcal{C}_{Lq|s}, \mathcal{P}_L, \chi_{\rm block}\right), \\ \rho_{\rm scar} &= (\Theta_{\rm scar}, Q_{\rm scar}, A_{\rm scar}/A_{\rm rd}). \end{aligned} \tag{81}$$

The precise conversion from each ρ_j to $\mathcal{R}_{\rm clock}$ is not universal. It must be fixed by channel-specific response models. What is universal at the level of this note is the methodological requirement: each channel must export either a residual estimate or a null bound in a form that can be compared.

A simple shared-normalization convention is to choose reference coefficients $\beta_j^{\rm ref} \neq 0$ and define

$$\widetilde{r}_j = \begin{cases} \rho_j/\beta_j^{\rm ref}, & \text{for scalar exports,} \\ \|\rho_j\|_{W_j}/\beta_j^{\rm ref}, & \text{for vector exports,} \end{cases} \tag{82}$$

where $\|\cdot\|_{W_j}$ is a predeclared weighted norm for vector-valued channels. Then each channel reports either an interval estimate for $\widetilde{r}_j$ or an upper bound

$$0 \le \widetilde{r}_j \le \widetilde{r}_{j,\max}. \tag{83}$$

This convention does not claim that all response coefficients are known a priori. It simply forces each channel to export to a common bookkeeping axis before any multi-channel interpretation is attempted.

The public protocol draft further separates *shape evidence* from *scale evidence*. For each channel j define a morphology score $M_j \in [0,1]$ and a normalized scale export $\widetilde{r}_j$. A channel is allowed to enter the shared residual fit only if

$$M_j \ge M_{j,\min} \tag{84}$$

under a predeclared nuisance projection. This prevents a weak amplitude fluctuation with the wrong morphology from being transported into the common residual ledger. The shared residual scale is then fitted only to morphology-admissible channels.

8.2 Joint consistency statistic

Suppose a subset of channels yields estimates $\widehat{r}_j$ of the same normalized residual scale with uncertainties σ_j. A minimal consistency statistic is

$$\chi^2_{\mathrm{clock}}(r) = \sum_{j\in J} \frac{(\widehat{r}_j - r)^2}{\sigma_j^2 + \sigma^2_{\mathrm{sys,j}}}, \tag{85}$$

where $\sigma_{\mathrm{sys,j}}$ is a declared systematic allowance. The best joint residual scale is

$$\widehat{r} = \arg\min_r \chi^2_{\mathrm{clock}}(r). \tag{86}$$

If most channels yield only upper bounds, then the joint allowed interval is

$$0 \le r \le \min_{j\in J} r^{(j)}_{\mathrm{max}}. \tag{87}$$

8.3 Cross-channel covariance

When repeated measurements or ensemble samples are available, the covariance structure is more informative than a single residual estimate. Let $\delta\rho_j$ be baseline-subtracted residual observables. A common residual scale predicts

$$\mathrm{Cov}(\delta\rho_i, \delta\rho_j) = \beta_i\beta_j \,\mathrm{Var}(\mathcal{R}_{\mathrm{clock}}) + \mathrm{Cov}(\eta_i, \eta_j). \tag{88}$$

If the channels have independent systematics, the nuisance covariance should be small or differently structured. A detected covariance pattern with the predicted signs and morphology would be more informative than a single-channel amplitude.

Diagnostic criterion 8.1 (Residual clock consistency)**.** A multi-channel residual interpretation is admissible only if the channel exports can be placed on a common residual scale without contradicting null bounds from other channels. It is strengthened if the baseline-subtracted residual observables show the covariance pattern predicted by (88).

8.4 What would be genuinely persuasive?

The most persuasive result would not be a large residual in one domain. It would be a sequence such as the following:

(X1) a small CMB feature template passes TT/TE/EE morphology tests but remains below discovery threshold;

(X2) a laboratory phase-clock experiment detects a drift–dephasing covariance with a compatible residual normalization;

(X3) a tunneling platform shows an opacity-linked clock/noise response with the same sign convention;

(X4) lattice lapse maps show topology-conditioned residual structure under a compatible normalization;

(X5) black-hole boundary data, if available, exhibit only a weak or bounded scar class consistent with the same residual scale.

Even this would not by itself prove the entire framework. But it would elevate the framework from a broad structural language to a quantitatively constrained cross-domain hypothesis.

9 Falsifiability Ledger

A broad framework must state what would count against it. The ledger in Table 5 summarizes the channel-specific observable, the framework-specific signature, and the meaning of a null result.

9.1 A sharper falsification standard

The framework should not be abandoned because one template fails. But it should be considered weakened if all of the following occur:

(F1) CMB transfer templates yield strong upper bounds over the natural scale-width range;

(F2) laboratory phase-clock tests show no drift–dephasing covariance under controlled residual drives;

(F3) tunneling systems show no opacity-linked response in any declared traversal-time proxy;

(F4) lattice lapse maps contain no topology-conditioned information beyond action density;

(F5) boundary-scar searches find no mass/spin-scaled residual class;

(F6) no common residual normalization can be transported across channels without contradiction.

This is the strongest form of falsifiability for a cross-domain structural framework.

10 Priority Roadmap

The most efficient development order is not to pursue the most spectacular claim first. It is to build the most controllable and falsifiable modules first, then connect them through the residual ledger.

10.1 Recommended order

The recommended order is

$$\begin{aligned}\text{CMB pseudo-likelihood} &\to \text{phase-clock lab protocol} \to \text{microscopic tunneling diagnostic} \\ &\to \text{lattice lapse-map implementation} \to \text{black-hole scar scaling.}\end{aligned} \tag{89}$$

Step 1: CMB pseudo-likelihood. The CMB channel already has public tools, public data, and clear observables. The first deliverable should be a grid of δC_ℓ^{TT}, δC_ℓ^{TE}, and δC_ℓ^{EE} templates, followed by injection-recovery and a preliminary bound on $\epsilon_{\rm clock}$.

Step 2: phase-clock lab protocol. The laboratory phase-clock test is the most controlled experimental route. The immediate goal is not a detection, but a protocol paper or technical note specifying the phase variable, residual drive, filter function, covariance vector, and null-bound extraction.

Step 3: microscopic tunneling diagnostic. The tunneling section should be developed after the phase-clock protocol because the cleanest tunneling platforms are also phase-clock platforms. Josephson junctions and STM-style barriers are natural candidates.

Step 4: lattice lapse-map implementation. The lattice module should be implemented as reproducible code. The first target is not proof of a mass gap or a new field-theoretic theorem; it is a stable map statistic that separates topology-conditioned lapse information from action-density artifacts.

Table 5: Falsifiability ledger for the prediction channels. The null-result column is essential: each channel must produce exclusion information even without a positive detection.

Prediction channel	**Observable**	**Framework-specific signature**	**Null result means**
CMB residual clock feature	$C_\ell^{TT}, C_\ell^{TE}, C_\ell^{EE}$	Correlated TT/TE/EE transfer morphology from one residual template $(\epsilon_{\rm clock}, k_*, \sigma_*)$.	Bound on $\lvert\epsilon_{\rm clock}\rvert$ for each template scale and width.
Laboratory phase-clock	$\delta\nu/\nu$, $\Gamma_{\rm res}$, $\Delta S_{\rm res}$	Frequency drift, dephasing, and entropy proxy co-vary under a common residual phase drive.	Bounds on $\lambda_\nu \mathcal{R}_{\rm lab}$ and $\lambda_\Gamma \mathcal{R}_{\rm lab}$.
Quantum tunneling	$\mathcal{T}$, $\tau_{\rm op}$, $S^{\rm res}_{\phi\phi}$, $\Gamma_{\rm deph}$	Opacity controls transmission plus declared clock/noise/dephasing proxies; WKB transmission is recovered.	No barrier-clock response in the selected time observable and opacity range.
Lattice lapse-map	$L_E(x,\tau)$, $q(x,\tau)$, $s(x,\tau)$, block charges	Low-lapse regions carry topology-conditioned information beyond action density and persist under flow.	Tested map $R_E \mapsto L_E$ lacks stable residual topology content.
Black-hole boundary scar	$\Theta_{\rm scar}$, $Q_{\rm scar}$, $A_{\rm scar}/A_{\rm rd}$	Residual post-ringdown features cluster in dimensionless mass/spin-scaled variables.	No accessible scar class above the amplitude and timing threshold.
Cross-channel consistency	Shared residual scale $\mathcal{R}_{\rm clock}$	One residual normalization is compatible with several channel exports and their covariance signs.	Framework becomes underconstrained or channel-inconsistent in the tested regime.

Step 5: black-hole scar scaling. The black-hole channel should remain downstream. It is valuable as a scaling criterion, but it should not be the first empirical pillar because event data, waveform systematics, and look-elsewhere effects make the channel fragile.

10.2 Concrete v0.5 targets

This public protocol draft has completed the first implementation layer and public-cleanup pass. A useful v0.5 pass should add the following next-step items:

(V5-1) run a real Boltzmann-code template grid and replace the schematic CMB curves by numerical $TT/TE/EE$ responses;

(V5-2) choose one laboratory platform and write a platform-specific protocol with expected sensitivity numbers;

(V5-3) fix the first tunneling platform and compute $t(E)$, $\tau_\varphi(E)$, and the opacity ledger in a concrete barrier model;

(V5-4) implement the lattice pseudocode on synthetic or public test configurations and report null-control distributions;

(V5-5) create a synthetic gravitational-wave event catalog and verify scar-class recovery and false-positive rates;

(V5-6) turn the residual export rule into a small machine-readable ledger format for channel bounds and morphology scores.

10.3 Conclusion

The prediction layer of the Residual Clock–Energy framework should be judged by compression, not by rhetoric. If each proposed signature requires an independent parameter, the framework adds little. If a single residual clock-sector normalization can constrain CMB morphology, laboratory phase drift, tunneling clock response, lattice lapse topology, and boundary-scar scaling, then the framework becomes a genuine cross-channel hypothesis.

This protocol note therefore converts the broad residual clock-energy idea into a concrete experimental program. It states what should be measured, what counts as a discriminating prediction, what null results mean, and how separate channels can be joined into a residual consistency ledger.

Acknowledgement of Scope

This document is a prediction and diagnostic note. It should not be read as a proof of the microscopic completion of the Residual Clock–Energy framework, as a claim of CMB anomaly detection, as a replacement for standard quantum mechanics, or as an observational claim about black-hole boundary scars. Its purpose is to make the framework easier to test by translating broad structural ideas into measurable channels, null bounds, and cross-channel consistency requirements.

References

[1] B. Lee, *From the Neutron-Lattice Thought Experiment to Residual Clock–Energy: A Chronological Guide to the Development of the Framework*, Version v0.2, Zenodo record, 2026. DOI: 10.5281/zenodo.19842618.

[2] B. Lee, *Operational Time and Residual Energy: A Structural Introduction to Clock–Generator Duality and Gauge–Gravity Response*, Version v1.1, Zenodo record, 2026. DOI: 10.5281/zenodo.19802122.

[3] B. Lee, *The Time Arrow in a Residual Clock Sector: Mathematical Closure, Numerical Diagnostics, and CMB Transfer Curves*, Zenodo record, 2026. DOI: 10.5281/zenodo.19840721.

[4] B. Lee, *Black-Hole Operational-Time Boundaries: Residual Lapse, Regulated Generators, and Boundary Data*, Zenodo record, 2026. DOI: 10.5281/zenodo.19809661.

[5] Planck Collaboration, *Planck 2018 results. VI. Cosmological parameters*, Astronomy & Astrophysics **641**, A6, 2020.

[6] Planck Collaboration, *Planck 2018 results. X. Constraints on inflation*, Astronomy & Astrophysics **641**, A10, 2020.

[7] X. Chen, *Primordial features as evidence for inflation*, Journal of Cosmology and Astroparticle Physics **2012**(01), 038, 2012.

[8] A. Lewis, A. Challinor, and A. Lasenby, *Efficient computation of cosmic microwave background anisotropies in closed Friedmann-Robertson-Walker models*, Astrophysical Journal **538**, 473–476, 2000.

[9] D. Blas, J. Lesgourgues, and T. Tram, *The Cosmic Linear Anisotropy Solving System (CLASS). II. Approximation schemes*, Journal of Cosmology and Astroparticle Physics **2011**(07), 034, 2011.

[10] T. E. Hartman, *Tunneling of a wave packet*, Journal of Applied Physics **33**, 3427–3433, 1962.

[11] M. Büttiker and R. Landauer, *Traversal time for tunneling*, Physical Review Letters **49**, 1739–1742, 1982.

[12] M. Büttiker, *Larmor precession and the traversal time for tunneling*, Physical Review B **27**, 6178–6188, 1983.

[13] E. H. Hauge and J. A. Støvneng, *Tunneling times: a critical review*, Reviews of Modern Physics **61**, 917–936, 1989.

[14] B. D. Josephson, *Possible new effects in superconductive tunnelling*, Physics Letters **1**, 251–253, 1962.

[15] M. Tinkham, *Introduction to Superconductivity*, 2nd edition, McGraw–Hill, 1996.

[16] J. Clarke and A. I. Braginski (eds.), *The SQUID Handbook, Vol. I: Fundamentals and Technology of SQUIDs and SQUID Systems*, Wiley-VCH, 2004.

[17] K. G. Wilson, *Confinement of quarks*, Physical Review D **10**, 2445–2459, 1974.

[18] M. Lüscher, *Properties and uses of the Wilson flow in lattice QCD*, Journal of High Energy Physics **2010**, 071, 2010.

[19] B. P. Abbott et al., *Observation of Gravitational Waves from a Binary Black Hole Merger*, Physical Review Letters **116**, 061102, 2016.

[20] V. Cardoso and P. Pani, *Testing the nature of dark compact objects: a status report*, Living Reviews in Relativity **22**, 4, 2019.